Steady-State and Pre-steady-State Kinetic Analysis of *Mycobacterium smegmatis* Cysteine Ligase (MshC)†

Fan Fan,‡ Andreas Luxenburger,§ Gavin F. Painter,§ and John S. Blanchard*,‡

Department of Biochemistry, Albert Einstein College of Medicine, 1300 Morris Park Avenue, Bronx, New York 10461, and Carbohydrate Chemistry Team, Industrial Research Limited, Post Office Box 31-310, Lower Hutt, New Zealand

Received June 11, 2007; Revised Manuscript Received July 23, 2007

ABSTRACT: *Mycobacterium tuberculosis* and many other members of the Actinomycetes family produce mycothiol, i.e., 1-D-*myo*-inosityl-2-(*N*-acetyl-L-cysteinyl)amido-2-deoxy-α-D-glucopyranoside (MSH or AcCys-GlcN-Ins), to act against oxidative and antibiotic stress. The biosynthesis of MSH is essential for cell growth and has been proposed to proceed via a biosynthetic pathway involving four key enzymes, MshA−MshD. The MSH biosynthetic enzymes present potential targets for inhibitor design. With this as a long-term goal, we have carried out a kinetic and mechanistic characterization, using steady-state and pre-steady-state approaches, of the recombinant *Mycobacterium smegmatis* MshC. MshC catalyzes the ATP-dependent condensation of GlcN-Ins and cysteine to form Cys-GlcN-Ins. Initial velocity and inhibition studies show that the steady-state kinetic mechanism of MshC is a Bi Uni Uni Bi Ping Pong mechanism, with ATP binding followed by cysteine binding, release of PP_i, binding of GlcN-Ins, followed by the release of Cys-GlcN-Ins and AMP. The steady-state kinetic parameters were determined to be k_{cat} equal to 3.15 s^{-1}, and K_m values of 1.8, 0.1, and 0.16 mM for ATP, cysteine, and GlcN-Ins, respectively. A stable bisubstrate analogue, 5′-*O*-[*N*-(L-cysteinyl)sulfamonyl]adenosine, exhibits competitive inhibition versus ATP and noncompetitive inhibition versus cysteine, with an inhibition constant of ∼306 nM versus ATP. Single-turnover reactions of the first and second half reactions were determined using rapid-quench techniques, giving rates of ∼9.4 and ∼5.2 s^{-1}, respectively, consistent with the cysteinyl adenylate being a kinetically competent intermediate in the reaction by MshC.

Mycothiol (MSH or acetyl-Cys-GlcN-Ins), a conjugate of *N*-acetylcysteine (AcCys) and 1-D-*myo*-inosityl-2-amido-2-deoxy-α-D-glucopyranoside (GlcN-Ins), is the predominant low-molecular-weight thiol that protects actinomycetes against oxidative stress and cellular electrophilic toxins (*1*−*4*). Among actinomycetes, mycobacteria generate the highest intracellular levels of MSH (*5*). Studies have shown that *Mycobacterium smegmatis* mutants lacking MSH become more sensitive toward oxidizing agents, electrophiles, and antibiotics (*1*−*3*), indicating the critical role of MSH in the survival and pathogenicity of mycobacteria (*1*). The detoxification mechanism of electrophiles by MSH has been proposed (path a in Scheme 1) to involve the formation of a MSH *S* conjugate of the electrophile (*1*). The conjugate is rapidly cleaved into GlcN-Ins and the mercapturic acid by a MSH *S*-conjugate amidase (Mca). The GlcN-Ins is recycled into the MSH biosynthetic pathway, whereas the mercapturic acid is expelled from the cell. Unlike actinomycetes, eukaryotes and eubacteria produce glutathiol (GSH), suggesting the enzymes involved in the MSH biosynthetic pathway as potential and selective targets for antimicrobial chemotherapy.

It has been proposed that MSH is synthesized via a series of enzymatic reactions (*6*−*9*), as illustrated in path b of Scheme 1. In brief, the process is initiated by an *N*-acetylglucosamine transferase (MshA) to generate 3-phospho-GlcNAc-Ins, which is subsequently dephosphorylated to form GlcNAc-Ins by an unknown phosphatase (*9*). GlcNAc-Ins is subsequently deacetylated by MshB. The resulting GlcN-Ins is ligated with cysteine in a reaction catalyzed by a cysteine ligase, MshC. The Cys-GlcN-Ins is then acetylated by MshD, yielding MSH. To understand the role and affects of each enzyme in MSH production and drug resistance, mutant *M. smegmatis* strains with specific mutations or insertions in the *mshA*−*mshD* genes were selected or constructed (*2*, *3*, *10*−*13*). The *mshA* mutant strain showed enhanced sensitivity to hydrogen peroxide and rifampicin but increased resistance to isoniazid (*2*). Disruption of *mshB* resulted in a 90−95% decrease in MSH production and no increased resistance to isoniazid compared to the wild-type strain. Moreover, this mutant did not show significant differences in sensitivity toward oxidative stress-inducing or alkylating agents, as well as antibiotics including cerulenin, vancomycin, rifampicin, and erythromycin (*13*). This observation was rationalized by noting that Mca possesses a weak GlcNAc-Ins deacetylase activity, allowing for the slow biosynthesis of MSH in the absence of a functional MshB (*4*). Interestingly, both $MshA^-$ and $MshB^-$ mutant strains were observed to be ∼6-fold more resistant toward ethionamide compared to the wild-type strain (*13*). The *mshD*

† This work was supported by NIH Grant AI33696 to J.S.B. and a Fellowship from the Heiser Program for Research in Leprosy and Tuberculosis of The New York Community Trust to F.F.

* To whom correspondence should be addressed. Telephone: (718) 430-3096. Fax: (718) 430-8565. E-mail: blanchar@aecom.yu.edu.

‡ Albert Einstein College of Medicine.

§ Industrial Research Limited.

10.1021/bi7011492 CCC: $37.00
Published on Web 09/12/2007

Scheme 1: Proposed Detoxification Mechanism (Path a) and Biosynthetic Pathway by MSH (Path b)

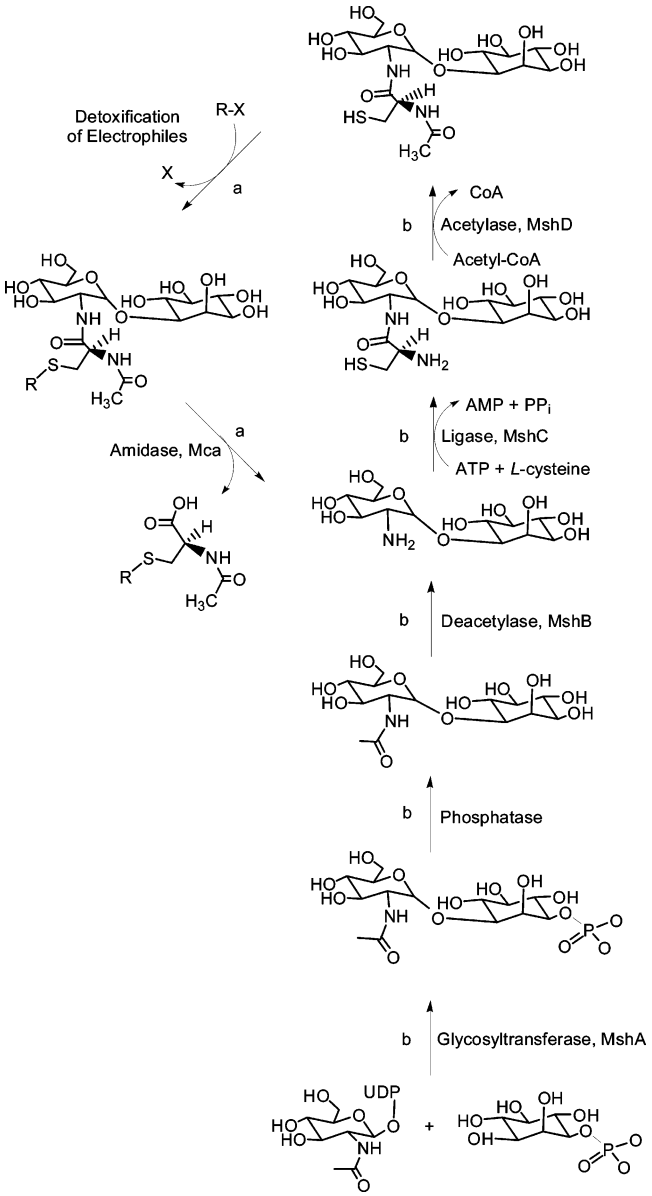

mutant exhibited similar sensitivities toward oxidative stress compared to wild-type strains. Intriguingly, two novel thiols, *N*-formyl-Cys-GlcN-Ins and *N*-succinyl-Cys-GlcN-Ins were observed in the *mshD* mutant, the latter of which was suggested to serve a similar function as MSH and thus account for the similar susceptibility to the wild type (*12*). Studies with a MshC mutant possessing ~80-fold less activity than that of the wild-type MshC showed significantly increased susceptibility toward oxidative and alkylating stress, as well as resistance to ethionamide and a broad range of antibiotics, including erythromycin, azithromycin, vancomycin, penicillin G, rifamycin, and rifampin (*3*). Similar to most MSH-deficient mutants, the *mshC* mutant also showed increased resistance to isoniazid compared to the wild type. A possible explanation by Rawat et al. suggests that MSH may be directly required to activate isoniazid (*3*).

MshC catalyzes the ATP-dependent ligation of cysteine to GlcN-Ins (Scheme 2). Despite its obvious significance, limited mechanistic, biochemical, or structural studies have been reported for MshC, unlike MshB and MshD, both of whose three-dimensional structures have been solved (*14*, *15*). Here, we report a detailed kinetic characterization of MshC from *M. smegmatis* using steady-state and pre-steady-state approaches.

MATERIALS AND METHODS

Materials. *Pfu* DNA polymerase was from Stratagene. pET28a(+) and the *Escherichia coli* strains, Rosetta2(DE3) and Top10, were obtained from Novagen. T4 DNA ligase and the restriction enzymes *Nde*I and *Eco*RI were from New England Biolabs. The oligonucleotide primers were synthesized by Invitrogen. Luria−Bertani broth was purchased from Fisher. All chromatographic materials were from Pharmacia. A protease inhibitor cocktail tablet [Complete, ethylenediaminetetraacetic acid (EDTA) free] was obtained from Roche. 5′-*O*-[*N*-(L-Cysteinyl)sulfamonyl]adenosine was from TriLink BioTechnologies. [^{14}C]-L-Cysteine and [α-^{33}P]ATP were purchased from Perkin-Elmer Life Sciences. PEI-F-thin-layer chromatography (TLC) and silica-TLC plates were obtained from EMD Chemicals, Inc. and Whatman Ltd., respectively. All other chemicals were purchased from Sigma or Aldrich.

Synthesis of GlcN-Ins. 1-*O*-(2-Amino-2-deoxy-α-D-glucopyranosyl)-D-*myo*-inositol (GlcN-Ins) was chemically synthesized from 2,3,4,5,6-penta-*O*-benzyl-D-*myo*-inositol (*16*) and methyl-2-azido-2-deoxy-3,4,5-tri-*O*-benzyl-1-thio-*β*-D-glucopyranoside.

1-*O*-(2-Amino-3,4,5-tri-*O*-benzyl-2-deoxy-α-D-glucopyranosyl)-2,3,4,5,6-penta-*O*-benzyl-D-*myo*-inositol was prepared as follows. Methyltriflate (2.81 mL, 24.8 mmol) was added dropwise to a stirred mixture of 2,3,4,5,6-penta-*O*-benzyl-D-*myo*-inositol (*16*) (5.22 g, 8.27 mmol), methyl-2-azido-2-deoxy-3,4,5-tri-*O*-benzyl-1-thio-*β*-D-glucopyranoside (4.18 g, 8.27 mmol), and 4 Å molecular sieves (ca. 4 g) in CH_2Cl_2 (130 mL) cooled to −25 °C. The reaction mixture was allowed to warm to room temperature over 4 h and then stirred at room temperature for a further 20 h when Et_3N (50 mL) was added. The mixture was filtered through celite, and the filter cake washed with ethyl acetate (2 × 200 mL). The combined filtrate was washed with water (400 mL) and brine (400 mL) and then dried ($MgSO_4$). After filtration, the solvent was removed *in vacuo* and the residue was purified by column chromatography on silica gel. Elution with EtOAc/light petroleum (from 1:6 to 1:4) afforded 1-*O*-(2-azido-3,4,5-tri-*O*-benzyl-2-deoxy-D-glucopyranosyl)-2,3,4,5,6-penta-*O*-benzyl-D-*myo*-inositol (6.30 g, 5.79 mmol, 70%) as an α,*β* mixture. This material was dissolved in diethyl ether (90 mL) and cooled to 0 °C, and lithium aluminum hydride (LAH, 1 M in diethyl ether, 12.3 mL, 12.3 mmol) was added dropwise over 2 min. After 1 h, the cold bath was removed and the reaction mixture was stirred at room temperature for 12 h when sodium−potassium tartrate (0.1 M, 300 mL) was added to quench the reaction. After the mixture was stirring for 30 min, it was extracted with ethyl acetate (3 × 200 mL) and the combined organic extract washed with brine (400 mL). After drying ($MgSO_4$) and filtration, the solvent was removed *in vacuo* and the residue was purified by column chromatography on silica gel. Elution with EtOAc/light petroleum (from 3:7 to 1:1) afforded 1-*O*-(2-amino-3,4,5-tri-*O*-benzyl-2-deoxy-α-D-glucopyranosyl)-2,3,4,5,6-penta-*O*-benzyl-D-*myo*-inositol (2.43 g, 2.29 mmol, 40%) as

Scheme 2

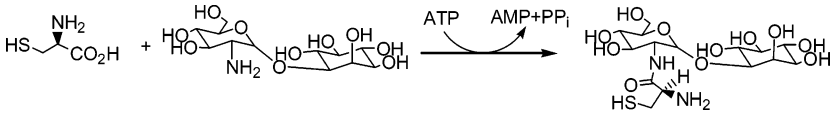

an oil. $[\alpha]_D^{22} = +44$ (*c* 0.50, $CHCl_3$). ^1H NMR (300 MHz, $CDCl_3$) δ: 7.39−7.07 (m, 40H), 5.17 (d, $J = 3.6$ Hz, 1H), 5.02−4.74 (m, 10H), 4.60−4.44 (m, 6H), 4.12−4.02 (m, 3H), 3.91−3.85 (m, 1H), 3.64−3.38 (m, 7H), 2.77 (dd, $J =$ 9.5, 3.6 Hz, 1H). ^{13}C NMR (75 MHz) δ: 39.2−38.0 (C, Ar), 128.4−127.3 (CH, Ar), 101.3, 84.1, 81.7, 81.2, 78.8, 78.6, 76.0, 75.9, 75.7, 75.3, 74.7, 74.5, 73.6, 72.8, 72.1, 68.8, 56.5. HRMS−ESI $[M+H]^+$ calcd for $C_{68}H_{72}NO_{10}$: 1062.5156. Found: 1062.5110. Anal. Calcd for $C_{68}H_{71}NO_{10}$: C, 76.88; H, 6.74; N, 1.32. Found: C, 77.16; H, 6.74; N, 1.33.

1-*O*-(2-Amino-2-deoxy-α-D-glucopyranosyl)-D-*myo*-inositol. Pd/C (10%, 600 mg) was added to a stirred solution of 1-*O*-(2-amino-3,4,5-tri-*O*-benzyl-2-deoxy-α-D-glucopyranosyl)-2,3,4,5,6-penta-*O*-benzyl-D-*myo*-inositol (1.09 g, 1.03 mmol) in ^{t}BuOH/H_2O/1 M HCl (61.0, 16.0, and 4.50 mL). The mixture was stirred under hydrogen for 14 h at room temperature, and the hydrogen was replaced with argon. The mixture was filtered through celite, and the pad was washed with H_2O (100 mL) and MeOH (100 mL). The combined filtrate was concentrated *in vacuo*, and the residue was purified by column chromatography on silica gel. Elution with ethyl acetate/MeOH/H_2O/AcOH (from 4:2:1:1 to 2:2:1:1) afforded the HCl salt of the product that was converted to the free base by chromatography on A26 amberlyst ion-exchange resin (hydroxide form) with H_2O. The solution was freeze-dried to afford 1-*O*-(2-amino-2-deoxy-α-D-glucopyranosyl)-D-*myo*-inositol (323 mg, 0.948 mmol, 92%) as a white powder. ^1H NMR (300 MHz, D_2O) δ: 5.09 (d, $J =$ 3.7 Hz, 1H), 4.18 (t, $J = 2.7$ Hz, 1H), 3.84−3.67 (m, 4H), 3.65−3.48 (m, 4H), 3.38 (t, $J = 9.5$ Hz, 1H), 3.28 (t, $J =$ 9.3 Hz, 1H), 2.72 (dd, $J = 10.2$, 3.74 Hz, 1H). ^{13}C NMR (75 MHz) δ: 101.8, 79.9, 74.6, 74.3, 73.1, 72.6, 72.4, 72.2, 71.6, 70.4, 61.2, 55.8. HRMS−ESI $[M + H]^+$ calcd for $C_{12}H_{24}NO_{10}$: 342.1400. Found: 342.1397. Anal. Calcd for $C_{12}H_{23}NO_{10}\cdot H_2O$: C, 40.11; H, 7.01; N, 3.90. Found: C, 39.78; H, 7.26; N, 3.71.

Cloning and Expression of M. smegmatis MshC. The *mshC* gene was amplified from *M. smegmatis* genomic DNA using *pfu* DNA polymerase and two primers (mshCf, 5′-ttttttcatatgatgcaatcgtggtcggcacc-3′ and mshCr 5′-ttttttgaattcttagaggtccacacccagcaacg-3′), containing *Nde*I and *Eco*RI restriction sites, respectively. The resulting amplicons were purified by 1% agarose gel electrophoresis using the QIAquick gel extraction kit following the protocol of the manufacturer. The amplified *mshC* gene and pET28a(+) vector were both subjected to endonuclease digestion for 3 h at 37 °C by *Nde*I and *Eco*RI, followed by a purification of the DNA by agarose gel. The *mshC* gene was then the ligated onto the pET28a-(+) plasmid by incubation at 16 °C overnight in the presence of T4-DNA ligase. A 2 μL aliquot of the ligation mixture was transformed directly into *E. coli* strain top 10 competent cells. The resulting colonies obtained by plating on Luria−Bertani agar plate containing 50 μg/mL ampicillin and 34 μg/mL chloramphenicol were screened for the presence of the *mshC* gene by *Nde*I and *Eco*RI digestion as described above. The nucleotide sequence of the construct was sequenced in both directions with both forward and reverse primers as described above.

A sequence-verified construct was transformed into Rosetta(DE3)2 for protein expression. A 10 mL preculture was used to inoculate 1 L of Luria−Bertani broth media containing ampicillin and chloramphenicol at final concentrations of 50 and 34 μg/mL, respectively. Cells were grown at 37 °C. When the optical density at 600 nm of the cell culture reached 0.8, isopropyl-β-D-thiogalactopyranoside (IPTG) was added into the culture to a final concentration of 0.5 mM and the temperature of the culture was lowered to 20 °C for overnight growth. Cells were harvested by centrifugation at 8000 rpm for 20 min at 4 °C and stored at −20 °C.

Purification and Assay of the Recombinant MshC. Unless otherwise stated, all of the purification steps were performed at 4 °C. The cell paste (typically ∼ 25 g) was resuspended with 50 mL of lysis buffer containing two protease inhibitor tablets, along with 0.2 mg/mL lysozyme, 0.1 mM phenylmethylsulfonyl fluoride (PMSF), 0.05 mg/mL DNase, 10 mM Mg^{2+}, 100 mM $(NH_4)_2SO_4$, 30 mM imidazole, and 20 mM tetraethylammonium chloride (TEA) at pH 7.9. The solution was incubated with stirring for 20 min. The resulting suspension was passed 3 times through a French Press and then centrifuged at 26800*g* for 10 min. The supernatant was loaded onto a 1.5 × 9 cm His-trap column, which was pre-equilibrated with 20 mM TEA, 20 mM imidazole, and 100 mM $(NH_4)_2SO_4$ at pH 7.9. Proteins were eluted with two gradients: a 30-column-volume gradient from 20 to 150 mM imidazole followed by a 3-column-volume gradient from 150 to 500 mM imidazole at a flow rate of 2 mL/min. The fractions with the highest purity as judged by sodium dodecyl sulfate−polyacrylamide gel electrophoresis (SDS−PAGE) were pooled and concentrated to ca. 3 mL using a YM 30 Amicon ultrafiltration membrane. The protein was then dialyzed against three changes of 20 mM TEA and 100 mM $(NH_4)_2SO_4$ at pH 7.9, centrifuged, and subsequently loaded onto a 1.5 × 70 cm Superdex 200 gel-filtration column. The enzyme was eluted at 0.5 mL/min, and the fractions were pooled and concentrated. After removal of precipitated protein by centrifugation, the enzyme was stored at −20 °C and was stable for at least 10 months.

Protein concentrations were determined using $\epsilon_{280} =$ 76 100 M^{-1} cm^{-1} for the native MshC with a 6-histidine tag. The concentration of enzyme was also determined using the Bio-Rad protein assay kit, with bovine serum albumin as the standard. The native molecular weight and oligomeric state was estimated using gel filtration on a column calibrated with Bio-Rad molecular-weight markers.

Enzyme Activity Assay. Initial velocities of the MshC reaction were assayed spectrophotometrically by coupling the formation of AMP to the reaction of myokinase, pyruvate kinase, and lactate dehydrogenase as described previously (*17*). The decrease in absorbance of reduced nicotinamide adenine dinucleotide (NADH) at 340 nm ($\epsilon_{340} = 6220$ M^{-1} cm^{-1}) was measured at 25 °C using a UVIKON 943 spectrophotometer with a circulating water bath and ther-

mospacers. The standard reaction contains 100 mM *N*-2-hydroxyethylpiperazine-*N*′-2-ethanesulfonic acid (HEPES) at pH 7.8, 10 mM $MgCl_2$, 10 mM ATP, 1 mM L-cysteine, 2 mM dithiothreitol (DTT), 100 μM GlcN-Ins, 1 mM potassium PEP, 300 μM NADH, 18 units of myokinase, 18 units of pyruvate kinase, and 18 units of lactate dehydrogenase in a total volume of 1 mL. After incubation for 5 min at 25 °C, reactions were initiated by the addition of MshC ($\leq$10 μL to a final concentration of ~25 nM). MshC enzymatic activities were corrected for the background activity, i.e., the decrease of absorbance at 340 nm caused by ATP hydrolysis. The rate of Cys-GlcN-Ins formation is proportional to the rate of NADH oxidation, where two molecules of NADH are oxidized for each molecule of Cys-GlcN-Ins formed.

Steady-State Kinetics. Initial velocity experiments were carried out at various concentrations of one substrate in the presence of different fixed levels of a second substrate and with the concentration of the third substrate kept saturating and constant. Product inhibition studies with pyrophosphate were performed at varying concentrations of ATP, 500 μM GlcN-Ins, and 40 μM or 2 mM cysteine. The bi-substrate analogue 5′-*O*-[*N*-(L-cysteinyl)sulfamonyl]adenosine was tested as an inhibitor versus ATP (at 50 μM cysteine and 100 μM GlcN-Ins) and cysteine (1 mM ATP and 100 μM GlcN-Ins), respectively.

Pre-steady-State Kinetics. Single-turnover experiments were performed at 25 °C using a KinTek rapid-quench apparatus (Model RQF-3) equipped with a constant temperature circulating water bath. The rates of the first half reaction (cysteine adenylation) were determined by rapidly mixing MshC containing 1 mM L-cysteine, 10 mM DTT, and 200 mM HEPES at pH 7.8, with a solution containing 0.1−4 mM [α-^{33}P]ATP (20 μCi/μmol), 10 mM $MgCl_2$, and 100 mM HEPES at pH 7.8. Control reactions exclude MshC from the reaction above. The reaction was incubated for a given time interval and then quenched with 110 μL of 150 mM EDTA. The enzyme was denatured by heat treatment in a boiling water bath for 1 min after quenching. After centrifugation, 1 μL of the reactions was spotted onto PEI TLC plates and radiolabeled ATP and AMP were resolved using 0.9 M guanidine hydrochloride as the mobile phase.

The rate of the second half reaction (cysteine ligation) was determined as described below. A solution containing 51 μM MshC, 20 mM $MgCl_2$, 2 mM ATP, 1 mM [^{14}C]-L-cysteine (50 μCi/μmol), 10 mM DTT, and 100 mM HEPES at pH 7.8 was preincubated at 25 °C for 5 min, allowing for the formation of the enzyme-bound cysteinyl adenylate intermediate, followed by rapid mixing with 40−1000 μM GlcN-Ins in 100 mM EDTA and 100 mM HEPES at pH 7.8. Control reactions contain water instead of GlcN-Ins. The reaction was incubated for a given time interval and then quenched with 110 μL of 3% TFA. The quenched solution was heated in a boiling water bath for 1 min and centrifuged to pellet denatured proteins. The solution was spotted onto silica TLC plates, and [^{14}C]-L-cysteine and [^{14}C]-L-cysteine-GlcN-Ins were separated using 3:1:1 CH_3CN/H_2O/28% NH_3 as the mobile phase. Both [^{33}P]AMP and [^{14}C]-L-cysteine-GlcN-Ins were quantitated using a Phosphorimager (Molecular Dynamics) and corrected for nonenzymatic activity.

Data Analysis. Parallel initial velocity patterns were fitted with eq 1, and intersecting patterns were fit to eq 2, where K_a and K_b are the Michaelis constants for the varied substrates A and B. Inhibition data were fitted to eqs 3−5 for competitive, uncompetitive, and noncompetitive inhibition patterns, respectively. *P* represents the concentration of the inhibitor (5′-*O*-[*N*-(L-cysteinyl)sulfamonyl]adenosine or pyrophosphate), and K_{is} and K_{ii} are the inhibition constants for the slope and intercept term, respectively.

$$\frac{v}{E} = \frac{k_{cat}AB}{K_bA + AB + K_{ia}K_b} \quad (1)$$

$$\frac{v}{E} = \frac{k_{cat}AB}{K_aB + K_bA + AB + K_{ia}K_b} \quad (2)$$

$$\frac{v}{E} = \frac{k_{cat}A}{K_a\left[1 + \left(\frac{P}{K_{is}}\right)\right] + A} \quad (3)$$

$$\frac{v}{E} = \frac{k_{cat}A}{K_a + A\left[1 + \left(\frac{P}{K_{ii}}\right)\right]} \quad (4)$$

$$\frac{v}{E} = \frac{k_{cat}A}{K_a\left[1 + \left(\frac{P}{K_{is}}\right)\right] + A\left[1 + \left(\frac{P}{K_{ii}}\right)\right]} \quad (5)$$

Single-turnover progress curve data were fitted to eq 6

$$Y = A(1 - e^{-k_{obs}t}) \quad (6)$$

For a two-step binding mechanism, the dependence of the single-exponential rate constant, k_{obs}, as a function of the substrate concentration is given by eq 7. For both half reactions by MshC, the intercept of k_{obs} versus substrate concentration curves appeared to be approximately zero. The data were thus fitted to eq 8, where $k_{off} = 0$.

$$k_{obs} = k_{max}[S]/(K_d + [S]) + k_{off} \quad (7)$$

$$k_{obs} = k_{max}[S]/(K_d + [S]) \quad (8)$$

RESULTS

Cloning, Expression, and Purification of MshC. To obtain large quantifies of MshC for kinetic characterization, the *M. smegmatis* mshC gene was cloned into plasmid pET28a(+) and expressed in *E. coli* Rosetta(DE3)2 cells. The heterologous expression by Rosetta(DE3)2 yielded large quantities of soluble MshC. MshC was purified using a combination of His-Trap affinity and gel-filtration chromatographies. The purification was monitored by SDS−PAGE, and these two columns were sufficient to achieve a catalytically active enzyme that was greater than 95% pure as judged by SDS−PAGE. Approximately 50 mg of purified enzyme was obtained per liter of culture. The subunit molecular mass of MshC determined by SDS−PAGE is ~47 kDa, consistent with the molecular weight of 47 562 Da calculated from the amino acid sequence of the *M. smegmatis* enzyme and the histidine tag. Superose 12 gel filtration was used to estimate

Table 1: Kinetic Parameters of *M. smegmatis* MshC

subtrate	K_m (mM)	k_{cat} (s^{-1})	k_{cat}/K_m (M^{-1} s^{-1})
ATP	1.84 ± 0.06	3.15 ± 0.18	1700 ± 100
cysteine	0.10 ± 0.01		31 500 ± 400
GlcN-Ins	0.16 ± 0.05		20 000 ± 600

the molecular weight of the native enzyme as 40 700 Da, suggesting that the native enzyme exist as a monomer.

Steady-State Kinetic Studies. The kinetic mechanism of *M. smegmatis* MshC was determined by initial velocity experiments using the coupled enzyme assay described above. The parallel lines revealed in double-reciprocal plots of the initial velocity using either ATP or cysteine and GlcN-Ins (Figure S1 in the Supporting Information) suggested a Ping Pong kinetic mechanism for MshC. The intersecting lines observed in double-reciprocal plots of the initial velocity by varying concentrations of ATP and cysteine and a fixed concentration of GlcN-Ins (Figure S1 in the Supporting Information) are indicative of the formation of a ternary E−ATP−cysteine complex. These data were fit to eq 1 or 2, yielding K_m values of ∼1.8, ∼0.1, and ∼0.16 mM for ATP, cysteine, and GlcN-Ins, respectively (Table 1). Pyrophosphate was used as a product inhibitor versus ATP and cysteine. When pyrophosphate was used versus ATP, an uncompetitive inhibition pattern was observed at a saturating concentration of cysteine, yielding a K_{ii} value of 1.9 ± 0.1 mM. When repeated at a nonsaturating concentration of cysteine, a noncompetitive pattern versus ATP was observed, yielding inhibition constants of 3.4 ± 1.0 and 3.7 ± 1.0 mM for K_{is} and K_{ii}, respectively (Figure 1). These data suggest that ATP binds to the enzyme prior to cysteine. 5′-*O*-[*N*-(L-Cysteinyl)sulfamonyl]adenosine was tested as a bisubstrate inhibitor because it is a structural analogue of the cysteinyl adenylate. 5′-*O*-[*N*-(L-Cysteinyl)sulfamonyl]adenosine acts as a competitive inhibitor versus ATP, with the competitive inhibition constant being 304 ± 40 nM, and as a noncompetitive inhibitor versus cysteine, with inhibition constants being 2.4 ± 0.2 μM for K_{is} and 390 ± 60 nM for K_{ii}, respectively (Figure 2). These data confirm the ordered binding of ATP and cysteine and are consistent with a Bi Uni Uni Bi Ping Pong kinetic mechanism as shown in Scheme 3.

Pre-steady-State Kinetic Analysis. The rate of cysteine−adenylate formation in the first half reaction was determined by single-turnover experiments using rapid-quench flow techniques with [α-^{33}P]ATP in the absence of GlcN-Ins. Plots of [α-^{33}P]AMP formation were obtained using different concentrations of [α-^{33}P]ATP (Figure 3A). The data were fit to eq 6 to obtain the rate constants at each concentration of ATP used. The rate constant for each reaction was subsequently plotted as a function of [ATP] (Figure 3B). The data were fit to eq 8 to obtain the maximum value of the rate constant, yielding a rate of cysteine−adenylate formation of 9.4 ± 0.7 s^{-1} and a K_d value for ATP of 1.7 ± 0.2 mM.

The rate of cysteine ligation in the second half reaction was measured in a similar manner to the first half reaction. In this reaction, ATP and [^{14}C]-L-cysteine were incubated with MshC for at least 5 min to allow for the complete formation of cysteinyl adenylate at the enzyme active site, followed by mixing with GlcN-Ins and EDTA, which was added to prevent additional turnover of the first half reaction after mixing with GlcN-Ins. Plots of Cys-GlcN-Ins formed versus time were generated using different concentrations of GlcN-Ins (Figure 4A). The data were fitted to eq 6 to obtain the rate constants at each concentration of GlcN-Ins used. The rate constant for each reaction was subsequently plotted as a function of [GlcN-Ins] (Figure 4B). The data were fitted to eq 8 to obtain the maximum value for the rate constant, yielding a rate of 5.2 ± 0.8 s^{-1} for the second half reaction and a K_d value for GlcN-Ins of 290 ± 90 μM.

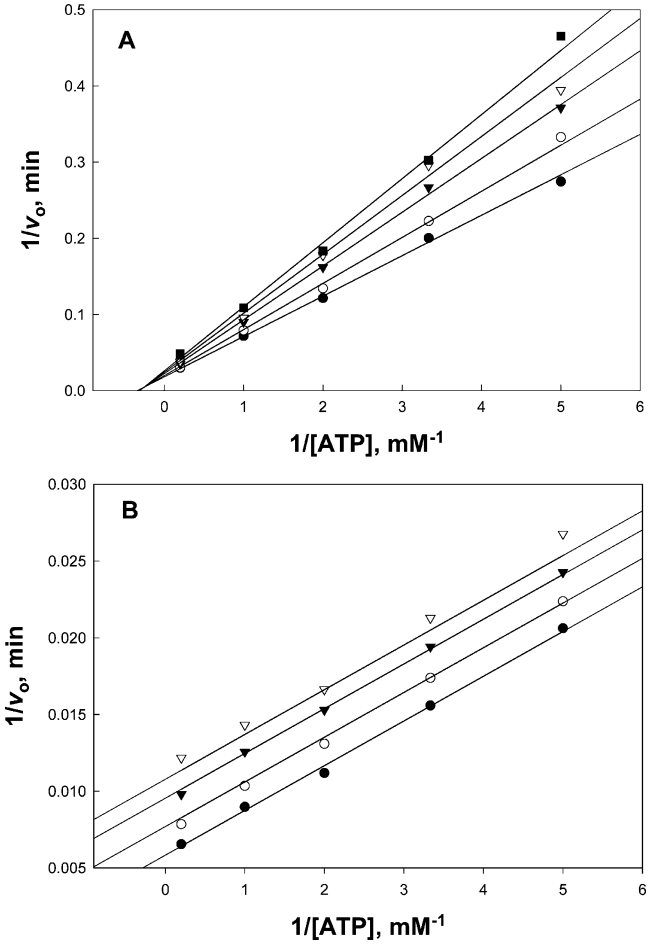

FIGURE 1: Product inhibition studies of MshC by pyrophosphate at 40 μM cysteine (A) and 2 mM cysteine (B). In A, assays were performed at 0 mM (●), 0.4 mM (○), 1 mM (▼), 1.4 mM (▽), and 1.8 mM (■) pyrophosphate. In B, assays were performed at 0 mM (●), 0.6 mM (○), 1.2 mM (▼), and 1.6 mM (▽) pyrophosphate. Activity assays were measured at 100 mM HEPES and 10 mM Mg^{2+} at pH 7.8 and 25 °C, as detailed in the Materials and Methods. The lines are fits of the data to eqs 5 and 4 for A and B, respectively.

DISCUSSION

Mycothiol plays important roles in the survival and pathogenicity of mycobacteria by its interactions with a broad spectrum of oxidants, electrophiles, as well as a number of antibiotics (*1*). As is the case for *Mycobacterium tuberculosis* Erdman, the *mshA* and *mshC* genes and presumably mycothiol are essential for the bacteria growth (*18*, *19*). The enzymes involved in MSH biosynthesis therefore present potential as drug targets for anti-mycobacterial treatment. Observations from the *M. smegmatis* strains with deficient or absent functions of MshA−MshD indicate that MshC has perhaps the greatest potential as a drug target, because

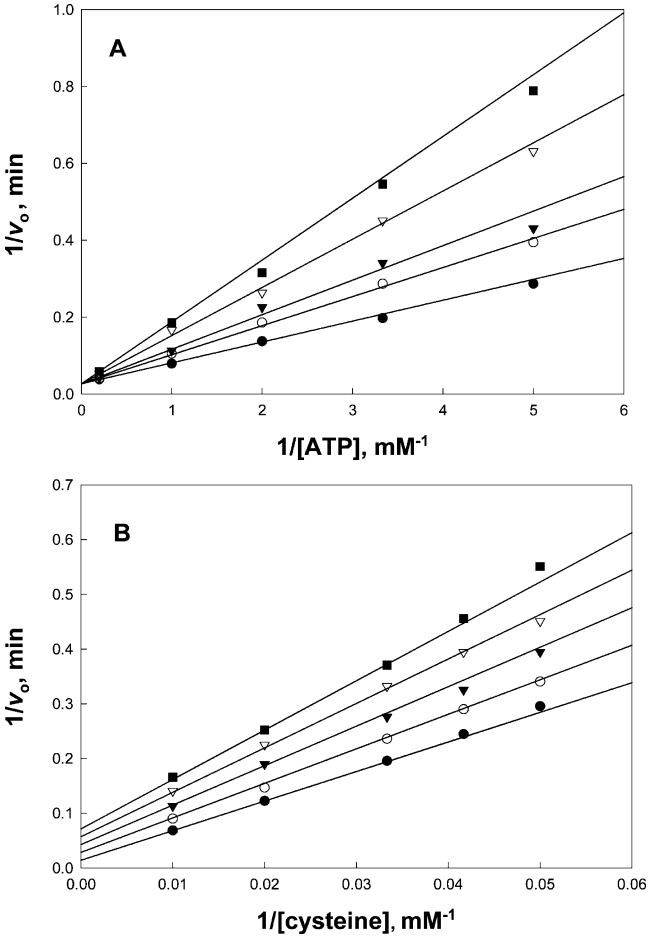

FIGURE 2: Inhibition studies of MshC with 5′-*O*-[*N*-(L-cysteinyl)-sulfamonyl]adenosine as the inhibitor. In A, initial velocities are at 0 nM (●), 120 nM (○), 200 nM (▼), 400 nM (▽), and 600 nM (■) 5′-*O*-[*N*-(L-cysteinyl)sulfamonyl]adenosine, 50 μM cysteine, and varying concentrations of ATP. In B, initial velocities are at 1 mM ATP, 0 nM (●), 400 nM (○), 800 nM (▼), 1200 nM (▽), and 1600 nM (■) 5′-*O*-[*N*-(L-cysteinyl)sulfamonyl]adenosine, and varying concentrations of cysteine. Activity assays were measured at 100 mM HEPES and 10 mM Mg^{2+} at pH 7.8 and 25 °C, as detailed in the Materials and Methods. The lines are fits of the data to eqs 3 and 5 for A and B, respectively.

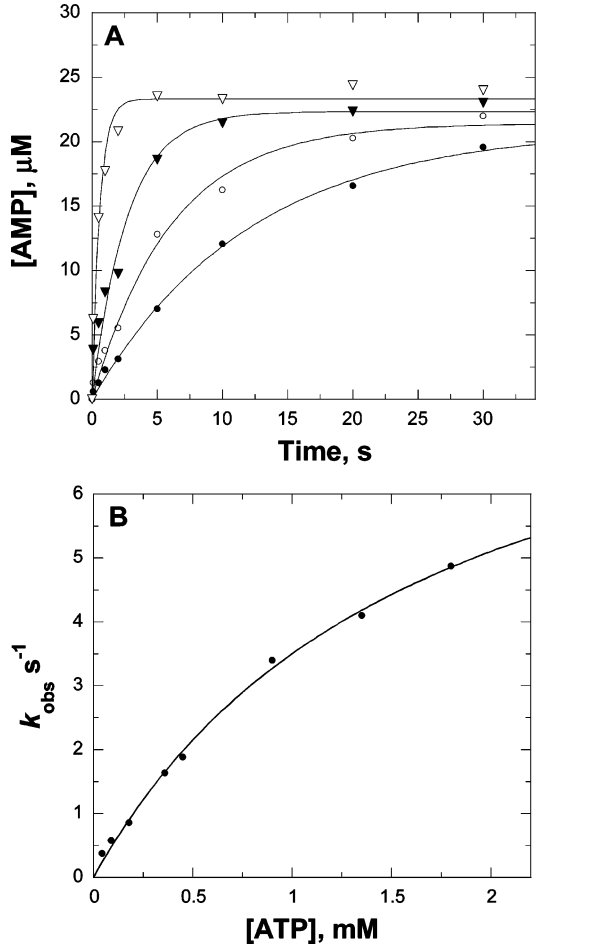

FIGURE 3: Pre-steady-state kinetics of AMP formation in the first half reaction of MshC. (A) Single-turnover time courses for the AMP formation. The curves shown are at representative ATP concentrations of 0.045 mM (●), 0.09 mM (○), 0.45 mM (▼), and 1.35 mM (▽). (B) Plot of the determined rate constants as a function of the ATP concentration used. Assays were carried out as described in the Materials and Methods. The curves are fits of the data to eqs 6 and 8 for A and B, respectively.

inhibiting MshC function results in strains with a higher susceptibility toward conventional antibiotic treatment (*2*, *3*, *10*−*13*). Despite its significance, only preliminary kinetic measurements have been reported for the *M. smegmatis* enzyme (*20*). Here, we present a detailed kinetic and mechanistic characterization of MshC from *M. smegmatis* as the first step for rationale inhibitor design.

Steady-State Kinetic Mechanism. The results from initial velocity and product, as well as bisubstrate analogue, inhibition studies of MshC are fully consistent with a Bi Uni Uni Bi Ping Pong kinetic mechanism as illustrated in Scheme 3. ATP binds to free enzyme followed by the binding of cysteine, forming a ternary E−ATP−cysteine complex. The enzyme releases pyrophosphate, with the formation of cysteine−adenylate bound in the enzyme active site. GlcN-Ins binds to the enzyme, and the amide bond between GlcN-Ins and cysteine is formed with the cleavage of the adenylate anhydride. The resulting Cys-GlcN-Ins and AMP are then released from the enzyme active site. The order of product release of AMP and Cys-GlcN-Ins was not defined in this study. Product inhibition by AMP versus ATP could not be determined because of the coupling enzyme assay used. However, we suggest that the enzyme releases Cys-GlcN-Ins prior to AMP based on kinetic studies with related aminoacyl-tRNA synthetases (*21*, *22*) and other ATP-dependent enzymes that catalyze amide-, ester-, and thioester-forming reactions (*17*, *23*, *24*). The reaction catalyzed by

Scheme 3

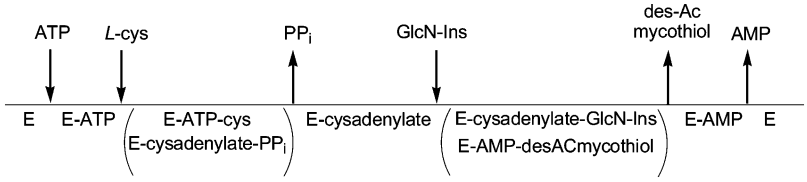

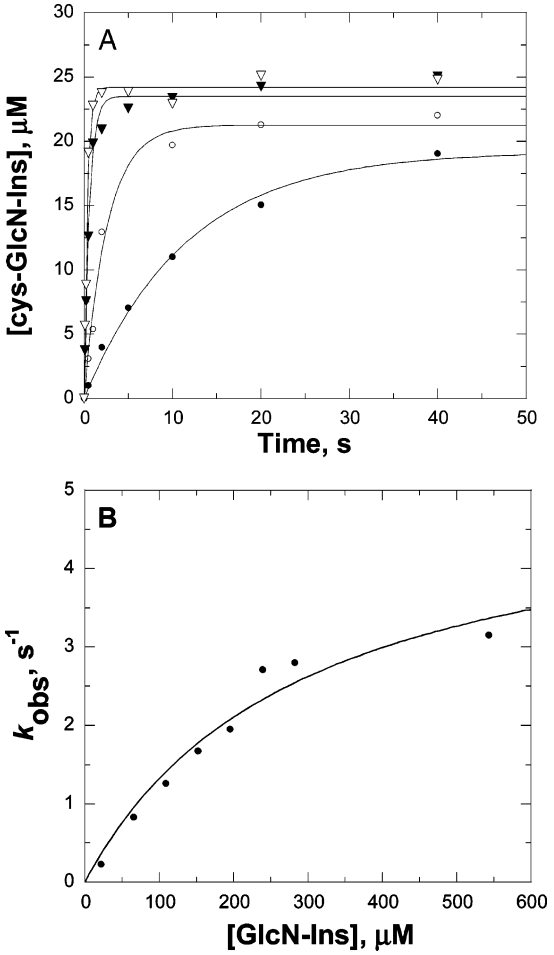

FIGURE 4: Pre-steady-state kinetics of AMP formation in the first half reaction of MshC. (A) Single-turnover time courses for the formation of Cys-GlcN-Ins. The curves are at representative GlcN-Ins concentrations of 21.8 μM (●), 65.5 μM (○), 152.2 μM (▼), and 239.1 μM (▽). (B) Plot of the determined rate constants as a function of the GlcN-Ins concentration used. Assays were carried out as described in the Materials and Methods. The curves are fits of the data to eqs 6 and 8 for A and B, respectively.

MshC can thus be divided into two half reactions: cysteine adenylation (or activation) and cysteine ligation (or condensation/transfer) (Scheme 4). Accordingly, the first reaction provides for carboxyl activation required for amide bond formation in the cysteine ligation reaction. The Bi Uni Uni Bi Ping Pong mechanism has been well-documented for other ATP-dependent synthetases, including pantothenate synthetase from *M. tuberculosis* (*17*), malonyl-CoA synthetase from *Bradyrhizobium japonicum* (*24*), fatty acyl-CoA synthetase from *E. coli* (*23*), as well as most of the aminoacyl-tRNA synthetases, including threonyl-tRNA synthetase from rat liver (*21*) and prolyl-tRNA synthetase from *E. coli* (*22*), although a study with *E. coli* threonyl-tRNA synthetase suggested a random binding of ATP and threonine to the enzyme (*25*). Aminoacyl-tRNA synthetases, however, can apparently use a variety of alternative kinetic mechanisms even though they all catalyze the same chemical reaction (*26*).

Pre-steady-State Kinetics. For any ping pong reaction, it is important to demonstrate that each of the two half reactions occur at rates greater than the determined steady-state rate. We therefore directly measured the rates of adenylate formation (first half reaction) as well as cysteine addition (second half reaction) and compared those to the overall reaction of MshC in the steady-state rate. In the first half reaction, cysteine reacts with ATP to form the cysteinyl adenylate and pyrophosphate at the enzyme active site in the absence of GlcN-Ins. The product, [^{33}P]AMP (produced from the breakdown of the cysteinyladenylate), and substrate, [^{33}P]ATP, were well-separated by TLC using 0.9 M guanidine hydrochloride as the mobile phase. The maximal rate constant of cysteine adenylate formation at saturating concentrations of ATP and cysteine was determined to be 9.4 $\pm$ 0.7 s^{-1}, which is 3 times greater than the overall reaction measured from steady-state kinetics. In addition, the rate of cysteine adenylate formation might be higher than $\sim$9.4 s^{-1} in the presence of GlcN-Ins, because the binding of GlcN-Ins may facilitate the rate of the first half reaction. An increasing rate of adenylation by the addition of the third substrate into the reaction mixture has been observed for argininosuccinate synthetase, for which the citrulline adenylation rate increases significantly by the addition of aspartate (*27*). This is however unlikely for MshC based on the calculations presented below.

The maximal rate of the second half reaction was also determined, using preincubation of ATP and cysteine with the enzyme to generate a stoichiometric enzyme−cysteinyladenylate complex. The maximal rate of cysteine ligation was determined to be 5.2 $\pm$ 0.7 s^{-1}, again higher than the steady-state k_{cat} value and consistent with the cysteine ligation half reaction being slower than the cysteine adenylation. A study carried out with pantothenate synthetase showed similar rate constants of pantothenate formation and the overall turnover, consistent with a slower amide bond formation than pantoyl adenylation formation (*17*). Similar results have also been reported for an isoleucyl-tRNA synthetase, where the rate of isolecyl-tRNA formation, measured from the mixing of tRNA to enzyme complexed with isoleucyl adenylate, is almost identical to k_{cat} (*28*).

The overall turnover of MshC is thus partially limited by both chemical steps. The steady-state value of k_{cat} can be calculated using eq 9, where k_{act} and k_{lig} represent the rate constants for cysteine activation and cysteine ligation, respectively. A steady state k_{cat} value of 3.3 s^{-1} can be calculated using eq 9 from the rate constants for cysteine activation and ligation of 9.4 and 5.2 s^{-1}, respectively. This compares quiet well to the k_{cat} value of 3.15 s^{-1} obtained from steady-state kinetic measurements.

$$k_{cat} = \frac{k_{act}k_{lig}}{k_{act} + k_{lig}} \quad (9)$$

Comparison with Aminoacyl-tRNA Synthetases. Because MshC shares significant sequence homology and catalyzes a similar reaction to cysteinyl-tRNA synthetase, mechanistic studies for aminoacyl-tRNA synthetases provide intriguing comparisons with MshC. Aminoacyl-tRNA synthetases can be divided into two classes, which differ in their structural folds and rate-limiting steps (*29*). The rate-limiting step in class I enzymes, including *E. coli* cysteinyl-tRNA and valinyl-tRNA synthetase, has been suggested to be product release (*29*), whereas for class II enzymes, adenylation or a combination of adenylation and aminoacyl transfer are suggested to be the rate-determining step(s). For example, both the rates of amino acid activation and aminoacyl transfer

Scheme 4

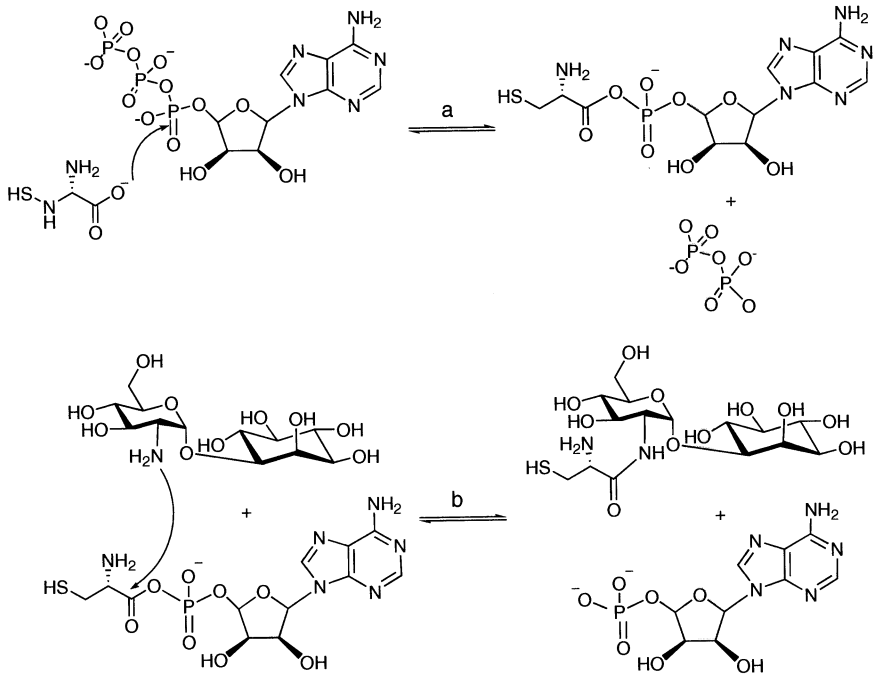

are approximately equal and rate-limiting for seryl- and phenylalanyl-tRNA synthetases (*30*, *31*). It is perhaps surprising that MshC differs from the homologous cysteinyl-tRNA in its rate-limiting steps. Structural modeling studies have suggested that elongation factor EF-Tu is able to form a complex with class I but not class II synthetases to assist product release (*29*). Recently, EF-Tu has been shown to associate with cysteinyl-tRNA synthetase, and EF-Tu affects the rate of aminoacylation by cysteinyl tRNA synthetase (*29*). In contrast, no enhancement of the rate for aminoacylation was observed in the class II alanyl-tRNA synthetase in the presence of EF-Tu (*29*). Additionally, tight binding of product cys-tRNA^{cys} to the enzyme was observed for cysteinyl-tRNA synthetase (*29*). Although direct experimental measurements have yet to be performed, cys-GlcN-Ins may bind to MshC less tightly because of its significantly decreased size compared to the cysteinylated-tRNA^{cys}, resulting in fewer interactions with the enzyme. The evolutionary relationship of MshC to cysteinyl-tRNA synthetase has been pointed out by Sareen et al. (*32*); however, additional mechanistic and structural studies are required to validate this hypothesis.

CONCLUSIONS

The essential nature of MSH biosynthesis in actinomycetes, the lack of these enzymes in mammals, and the hypersensitivity toward antibiotics observed for *M. smegmatis* strains lacking MshC activity suggest that MshC is an important target for inhibitor design. The kinetic mechanism was determined to be ordered Bi Uni Uni Bi Ping Pong using a combination of initial velocity, product, and bisubstrate inhibition studies. The namomolar binding of 5′-*O*-[*N*-(L-cysteinyl)sulfamonyl]adenosine to MshC suggests that this compound could be a starting scaffold for further elaboration. These studies have demonstrated that a kinetically competent cysteinyl−adenylate intermediate is formed in the first half reaction. The subsequent reaction of GlcN-Ins with the cysteinyl adenylate is slower. The overall k_{cat} value calculated from the individual maximal rates of the two half reactions is, within experimental error, equal to the k_{cat} values for the overall reactions determined in the steady state. These studies provide the necessary information for future rationale inhibitor design.

ACKNOWLEDGMENT

We thank Dr. James C. Errey for his help and support for the project, Dr. Matthew W. Vetting for his assistance in the determination of the oligomeric status of MshC, and Dr. Dave P Ballou for his thoughtful suggestion on the results of the pre-steady-state kinetics.

SUPPORTING INFORMATION AVAILABLE

Figure S1, the steady-state kinetic data with ATP, cysteine, or GlcN-Ins that were fit with both eqs 1 and 2. This material is available free of charge via the Internet at http://pubs.acs.org.

REFERENCES

1. Newton, G. L., Av-Gay, Y., and Fahey, R. C. (2000) A novel mycothiol-dependent detoxification pathway in mycobacteria involving mycothiol *S*-conjugate amidase, *Biochemistry 39*, 10739−10746.
2. Newton, G. L., Unson, M. D., Anderberg, S. J., Aguilera, J. A., Oh, N. N., delCardayre, S. B., Av-Gay, Y., and Fahey, R. C. (1999) Characterization of *Mycobacterium smegmatis* mutants defective in 1-D-*myo*-inosityl-2-amino-2-deoxy-α-D-glucopyranoside and mycothiol biosynthesis, *Biochem. Biophys. Res. Commun. 255*, 239−244.
3. Rawat, M., Newton, G. L., Ko, M., Martinez, G. J., Fahey, R. C., and Av-Gay, Y. (2002) Mycothiol-deficient *Mycobacterium smegmatis* mutants are hypersensitive to alkylating agents, free radicals, and antibiotics, *Antimicrob. Agents Chemother. 46*, 3348−3355.
4. Buchmeier, N. A., Newton, G. L., Koledin, T., and Fahey, R. C. (2003) Association of mycothiol with protection of *Mycobacterium tuberculosis* from toxic oxidants and antibiotics, *Mol. Microbiol. 47*, 1723−1732.

5. Newton, G. L., Arnold, K., Price, M. S., Sherrill, C., Delcardayre, S. B., Aharonowitz, Y., Cohen, G., Davies, J., Fahey, R. C., and Davis, C. (1996) Distribution of thiols in microorganisms: Mycothiol is a major thiol in most actinomycetes, *J. Bacteriol. 178*, 1990−1995.
6. Anderberg, S. J., Newton, G. L., and Fahey, R. C. (1998) Mycothiol biosynthesis and metabolism. Cellular levels of potential intermediates in the biosynthesis and degradation of mycothiol in *Mycobacterium smegmatis*, *J. Biol. Chem. 273*, 30391−30397.
7. Bornemann, C., Jardine, M. A., Spies, H. S., and Steenkamp, D. J. (1997) Biosynthesis of mycothiol: Elucidation of the sequence of steps in *Mycobacterium smegmatis*, *Biochem. J. 325* (part 3), 623−629.
8. Newton, G. L., and Fahey, R. C. (2002) Mycothiol biochemistry, *Arch. Microbiol. 178*, 388−394.
9. Newton, G. L., Ta, P., Bzymek, K. P., and Fahey, R. C. (2006) Biochemistry of the initial steps of mycothiol biosynthesis, *J. Biol. Chem. 281*, 33910−33920.
10. Koledin, T., Newton, G. L., and Fahey, R. C. (2002) Identification of the mycothiol synthase gene (*mshD*) encoding the acetyltransferase producing mycothiol in actinomycetes, *Arch. Microbiol. 178*, 331−337.
11. Newton, G. L., Koledin, T., Gorovitz, B., Rawat, M., Fahey, R. C., and Av-Gay, Y. (2003) The glycosyltransferase gene encoding the enzyme catalyzing the first step of mycothiol biosynthesis (mshA), *J. Bacteriol. 185*, 3476−3479.
12. Newton, G. L., Ta, P., and Fahey, R. C. (2005) A mycothiol synthase mutant of *Mycobacterium smegmatis* produces novel thiols and has an altered thiol redox status, *J. Bacteriol. 187*, 7309−7316.
13. Rawat, M., Kovacevic, S., Billman-Jacobe, H., and Av-Gay, Y. (2003) Inactivation of mshB, a key gene in the mycothiol biosynthesis pathway in *Mycobacterium smegmatis*, *Microbiology 149*, 1341−1349.
14. Vetting, M. W., Roderick, S. L., Yu, M., and Blanchard, J. S. (2003) Crystal structure of mycothiol synthase (Rv0819) from *Mycobacterium tuberculosis* shows structural homology to the GNAT family of *N*-acetyltransferases, *Protein Sci. 12*, 1954−1959.
15. Maynes, J. T., Garen, C., Cherney, M. M., Newton, G., Arad, D., Av-Gay, Y., Fahey, R. C., and James, M. N. (2003) The crystal structure of 1-D-*myo*-inosityl-2-acetamido-2-deoxy-α-D-glucopyranoside deacetylase (MshB) from *Mycobacterium tuberculosis* reveals a zinc hydrolase with a lactate dehydrogenase fold, *J. Biol. Chem. 278*, 47166−47170.
16. Aneja, R., Aneja, S., Pathak, V. P., and Ivanova, P. T. (1994) The absolute configuration of (+)-1,2,4,5,6-penta-*O*-benzyl-*myo*-inositol, *Tetrahedron Lett. 35*, 6061−6062.
17. Zheng, R., and Blanchard, J. S. (2001) Steady-state and pre-steady-state kinetic analysis of *Mycobacterium tuberculosis* pantothenate synthetase, *Biochemistry 40*, 12904−12912.
18. Buchmeier, N., and Fahey, R. C. (2006) The mshA gene encoding the glycosyltransferase of mycothiol biosynthesis is essential in *Mycobacterium tuberculosis* Erdman, *FEMS Microbiol. Lett. 264*, 74−79.
19. Sareen, D., Newton, G. L., Fahey, R. C., and Buchmeier, N. A. (2003) Mycothiol is essential for growth of *Mycobacterium tuberculosis* Erdman, *J. Bacteriol. 185*, 6736−6740.
20. Newton, G. L., Ta, P., Sareen, D., and Fahey, R. C. (2006) A coupled spectrophotometric assay for l-cysteine:1-D-*myo*-inosityl-2-amino-2-deoxy-α-D-glucopyranoside ligase and its application for inhibitor screening, *Anal. Biochem. 353*, 167−173.
21. Allende, C. C., Chaimovich, H., Gatica, M., and Allende, J. E. (1970) The aminoacyl transfer ribonucleic acid synthetases. II. Properties of an adenosine triphosphate-threonyl transfer ribonucleic acid synthetase complex, *J. Biol. Chem. 245*, 93−101.
22. Papas, T. S., and Mehler, A. H. (1971) Kinetic studies of the prolyl transfer ribonucleic acid synthetase of *Escherichia coli*. Order of addition of substrates and release of products, *J. Biol. Chem. 246*, 5924−5928.
23. Black, P. N., DiRusso, C. C., Sherin, D., MacColl, R., Knudsen, J., and Weimar, J. D. (2000) Affinity labeling fatty acyl-CoA synthetase with 9-*p*-azidophenoxy nonanoic acid and the identification of the fatty acid-binding site, *J. Biol. Chem. 275*, 38547−38553.
24. Kim, Y. S., and Kang, S. W. (1994) Steady-state kinetics of malonyl-CoA synthetase from *Bradyrhizobium japonicum* and evidence for malonyl-AMP formation in the reaction, *Biochem. J. 297* (part 2), 327−333.
25. Bovee, M. L., Pierce, M. A., and Francklyn, C. S. (2003) Induced fit and kinetic mechanism of adenylation catalyzed by *Escherichia coli* threonyl-tRNA synthetase, *Biochemistry 42*, 15102−15113.
26. Kisselev, L. L., and Favorova, O. O. (1974) Aminoacyl-tRNA synthetases: Some recent results and achievements, *Adv. Enzymol. Relat. Areas Mol. Biol. 40*, 141−238.
27. Ghose, C., and Raushel, F. M. (1985) Determination of the mechanism of the argininosuccinate synthetase reaction by static and dynamic quench experiments, *Biochemistry 24*, 5894−5898.
28. Eldred, E. W., and Schimmel, P. R. (1972) Investigation of the transfer of amino acid from a transfer ribonucleic acid synthetase-aminoacyl adenylate complex to transfer ribonucleic acid, *Biochemistry 11*, 17−23.
29. Zhang, C. M., Perona, J. J., Ryu, K., Francklyn, C., and Hou, Y. M. (2006) Distinct kinetic mechanisms of the two classes of aminoacyl-tRNA synthetases, *J. Mol. Biol. 361*, 300−311.
30. Dibbelt, L., Pachmann, U., and Zachau, H. G. (1980) Serine activation is the rate limiting step of tRNASer aminoacylation by yeast seryl tRNA synthetase, *Nucleic Acids Res. 8*, 4021−4039.
31. Dibbelt, L., and Zachau, H. G. (1981) On the rate limiting step of yeast tRNAPhe aminoacylation, *FEBS Lett. 129*, 173−176.
32. Sareen, D., Steffek, M., Newton, G. L., and Fahey, R. C. (2002) ATP-dependent L-cysteine:1-D-*myo*-inosityl-2-amino-2-deoxy-α-D-glucopyranoside ligase, mycothiol biosynthesis enzyme MshC, is related to class I cysteinyl-tRNA synthetases, *Biochemistry 41*, 6885−6890.

BI7011492